This is the peer reviewed version of the following article:

Localized Water-In-Salt Electrolyte for Aqueous Lithium-Ion Batteries

Journal title; **Angewandte Chemie**

First published**: 26 Jul 2021**

which has been published in final form at

https://onlinelibrary.wiley.com/doi/10.1002/ange.202107389

This article may be used for non-commercial purposes in accordance with Wiley Terms and Conditions for Use of Self-Archived Versions.

This article may not be enhanced, enriched or otherwise transformed into a derivative work, without express permission from Wiley or by statutory rights under applicable legislation. Copyright notices must not be removed, obscured or modified. The article must be linked to Wiley's version of record on Wiley Online Library and any embedding, framing or otherwise making available the article or pages thereof by third parties from platforms, services and websites other than Wiley Online Library must be prohibited.

"Localized Water-In-Salt" Electrolyte for Aqueous Lithium-Ion Batteries

Pauline Jaumaux [a†], Xu Yang [a†], Bao Zhang[b,c], Javad Safaei[a], Xiao Tang[a], Dong Zhou[a*], Chunsheng Wang[b*], Guoxiu Wang[a*]

Abstract: "Water-in-salt" (WIS) electrolytes using super-concentrated organic lithium (Li) salts are attracting tremendous interest for high energy aqueous Li-ion batteries, owing to their wide electrochemical stability window that enables the application of high-energy electrode couples. However, the high salt cost, high viscosity, poor wettability and environmental hazards remain a great challenge. Herein, we present a "localized water-in-salt" (LWIS) electrolyte based on low-cost lithium nitrate ($LiNO_3$) salt and 1,5-pentanediol (PD) as inert diluent. The addition of PD not only maintains the solvation structure of the WIS electrolyte and improves the electrolyte stability via hydrogen-bonding interactions with water and NO_3^- molecules, but also dramatically reduces the total salt concentration. Furthermore, by in-situ gelling the LWIS electrolyte with tetraethylene glycol diacrylate (TEGDA) monomer, the electrolyte stability window can be further expanded to 3.0 V. The as-developed Mo_6S_8|LWIS gel electrolyte|$LiMn_2O_4$ (LMO) batteries delivered outstanding cycling performance with an average Coulombic efficiency of 98.53 % after 250 cycles at 1 C.

Introduction

Rechargeable lithium (Li)-ion batteries have dominated the energy storage market from portable electronics to electric vehicles in the past two decades due to their high energy density and long cycle life.[1] However, the prevailing application of non-aqueous electrolytes based on flammable and toxic organic solvents (*e. g.* carbonates and ethers) in Li-ion batteries has triggered severe safety hazards, including fire, explosion and harmful leakage.[2] Replacing these non-aqueous electrolytes with aqueous electrolytes not only can efficiently eliminate the safety issues of Li-ion batteries, but also reduce the battery manufacturing costs due to the non-reliance on ultra-dry assembly facilities.[3] Nonetheless, the electrochemical stability window (<2 V) of traditional dilute aqueous electrolytes is too narrow to support high-energy electrochemical couples, which is a major bottleneck for the development of aqueous Li-ion batteries.[4]

In 2015, "water-in-salt" (WIS) electrolytes were developed to unprecedentedly expand the electrochemical window of aqueous electrolytes, in which the dissolved Li salts far outnumber water molecules by both volume and mass.[5] A protective solid electrolyte interphase (SEI) was constructed on the anode surface in a 21 m (mol $kg^{-1}_{solvent}$) lithium bis(trifluoromethane)sulfonimide (LiTFSI) aqueous electrolyte which exhibited a 3.0 V-wide stability window. Other organic Li salts, *e. g.* lithium bis(pentafluoroethanesulfonyl)imide[6], lithium trifluoromethane sulfonate[7] and lithium (trifluoromethanesulfonyl)(pentafluoroethanesulfonyl)imide[8], have been introduced to the WIS electrolytes to further improve the saturation limitation of salts and thus further widen the electrochemical window. In addition, a co-solvent (*e. g.* ether[9] and carbonate[10]) was also introduced into WIS electrolyte to promote the SEI formation. However, the super-high concentration of these toxic Li salts in WIS electrolytes raises new concerns of high cost, high viscosity, poor wettability toward electrodes, and environmental hazards.[11]

To overcome above intrinsic challenges of WIS electrolytes, herein, we (1) used inexpensive and eco-friendly inorganic Li salts to replace the toxic and costly organic Li salts, and (2) lowered the electrolyte salt concentration by diluting the WIS electrolytes with an inert solvent (called a "diluent") that dissolves the water but not the inorganic salt. Therefore, the diluent does not alter the salt solvation structure of WIS electrolytes forming a "localized water-in-salt (LWIS)" electrolytes. Since the organic diluent has a much wider electrochemical stability window than water-in-salt electrolyte, the LWIS are expected to preserve (or even enhance) the electrochemical stability of WIS electrolytes while reducing the salt concentration, decreasing the viscosity and improving the wettability. The salt/diluent configuration for LWIS electrolytes have not been reported to our best knowledge. To demonstrate the concept of LWIS, we used lithium nitrate ($LiNO_3$) as Li salt and 1,5-pentanediol (PD) as diluent. The application of PD not only significantly lowers the total Li salt concentration of WIS electrolyte, but also reduces the water reactivity in HER/OER via hydrogen-bonding interactions between PD with water molecules and NO_3^- anions, thus enabling an electrochemical stability window of ≈2.8 V (partly attributed to the formation of SEI on the anode surface). Furthermore, by *in-situ* polymerizing of tetraethylene glycol diacrylate (TEGDA) monomer in the LWIS electrolyte, the as-prepared aqueous gel electrolyte exhibited an enhanced electrolyte stability of ≈3.0 V without flammability or liquid leakage hazard. The as-developed Mo_6S_8|LWIS gel electrolyte|$LiMn_2O_4$ (LMO) battery showed a high cycling stability with 98.53 % Coulombic efficiency at 1C. The design principles for LWIS electrolytes reported in this work will boost the future development of high-energy and low-cost aqueous Li-ion batteries.

Results and Discussion

Salt/diluent screening for a wide electrochemical stability window

According to the design concept of LWIS electrolytes, an ideal diluent should simultaneously possess: (1) high miscibility with

[a] P. Jaumaux, X. Yang, J. Safaei, X. Tang, Dr. D. Zhou, Prof. G. Wang
Centre for Clean Energy Technology, School of Mathematical and Physical Sciences
University of Technology Sydney
Sydney, NSW 2007 (Australia)
E-mail: zhoudong087@gmail.com, Guoxiu.Wang@uts.edu.au

[b] Dr. B. Zhang, Prof. C. Wang
Department of Chemical and Biomolecular Engineering, University of Maryland, College Park, Maryland 20742, United States
E-mail: cswang@umd.edu

[c] School of Optical and Electronic Information, Huazhong University of Science and Technology, Wuhan, 430074, P. R. China

† These authors contributed equally to this work.

water; (2) low Li salt solubility and (3) wider chemical and electrochemical stability with electrodes during the battery operation.[12] We compared the miscibility of different solvents with water in a mass ratio 1: 1. As shown in **Figure 1**a, diethylene carbonate (DEC), fluoroethylene carbonate (FEC) and propylene carbonate (PC) formed bi-phasic mixtures with water, while tetraethylene glycol dimethyl ether (TEGDME) formed an emulsion in water. In contrast, ethylene carbonate (EC) and PD can be well-mixed with water without phase separation (**Figure 1**a), and offer wider electrochemical stability window (4.2 V) than WIS (3.0 V) as shown in **Figure S1,** which is in the working voltage range of batteries.[13] Therefore, EC and PD can act as diluent candidates. Furthermore, the solubilities of LiTFSI as a representative organic Li salt and $LiNO_3$ as a representative inorganic Li salt in different solvents at 25 °C are also presented in **Figure 1**b. It should be noted that these solubility values represent the solubility limits of stable supersaturated solutions which were prepared by dissolving the Li salt at 40 °C and then cooling down to 25 °C. It is seen that LiTFSI delivers high solubility in both water (21 m) and organic diluents (*i. e.* 8.0 m in EC and 6.5 m in PD). For comparison, inorganic $LiNO_3$ salt is highly soluble in water (25 m), but has poor solubility in diluents (*i. e.* 0.87 m in EC and 0.75 m in PD). This solubility difference of inorganic Li salts makes them suitable candidates to develop LWIS electrolytes.[14] Moreover, we measured the solubilities of various inorganic Li salts, including lithium chloride (LiCl), lithium sulfate (Li_2SO_4), lithium phosphate (Li_3PO_4) and lithium acetate (LiAc), in water and PD diluent. As seen from **Figure 1**c, although all the inorganic Li salts exhibit low solubilities of <2 m in PD, the water solubility of $LiNO_3$ (25 m) far exceeds other Li salts (LiCl: 24.1 m; LiAc: 11.1 m; Li_2SO_4: 3.2 m; Li_3PO_4: 0.2 m). Consequently, $LiNO_3$ was chosen as the ideal Li salt to form a LWIS electrolyte. The $LiNO_3$ -based aqueous electrolytes is weakly acidic with pH values comparable to LiTFSI-based electrolytes (**Figure S2**).

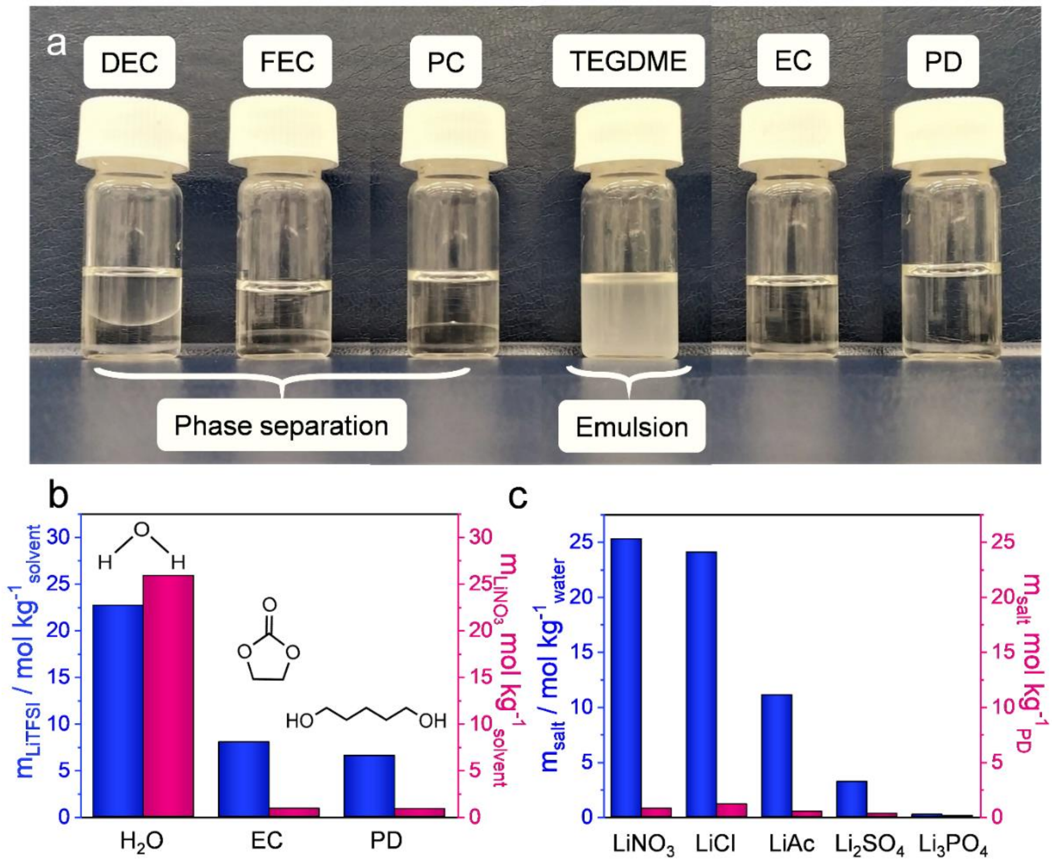

Figure 1. (**a**) Illustration of the miscibility of different solvents with water in a 1: 1 mass ratio. (**b**) Solubilities of LiTFSI (blue) and $LiNO_3$ (pink) in different solvents at 25 ℃. (**c**) Solubilities of different Li salts in water (blue) and PD (pink) at 25 ℃

The electrochemical stability windows of the $LiNO_3$-based LWIS and WIS electrolytes were evaluated by cyclic voltammetry (CV) in a three-electrode cell with titanium (Ti) mesh as working electrode, platinum (Pt) wire as counter electrode and Ag/AgCl as reference electrode. **Figure S3** shows the first and second CV curves of the 25 m $LiNO_3$ in H_2O WIS electrolyte, 12.5 m $LiNO_3$ in H_2O: PD (1: 1 by mass) LWIS electrolyte and LWIS gel electrolyte (prepared by *in-situ* polymerizing 6 wt% TEGDA monomer in 12.5 m $LiNO_3$ in H_2O: PD electrolyte). The electrochemical window values of LWIS and LWIS gel electrolytes from the 2nd CV cycle were obviously larger than those in the 1st cycle, while the electrochemical stability windows showed almost no change during cycling in the 12.5 m and 25 m $LiNO_3$ in H_2O electrolytes. This seems to be mainly due to the SEI formation that suppresses the hydrogen evolution reaction (HER) in two LWIS aqueous electrolytes,[15] which will be discussed in the following part. The impact of dilutes (EC and PD) on electrochemical stability window of LWIS electrolytes was also investigated. **Figure 2** and **Figure S4** shows the 2nd linear polarization profiles of the electrolytes with and without dilute. The 10.5 m LiTFSI in H_2O electrolyte exhibited a stability window of 2.1 V (**Figure 2**a). In this electrolyte, Li ions are solvated by water molecules to form solvation sheaths, meanwhile anions are mostly excluded from these solvation sheaths (**Figure 2**e, left panel).[5, 16] After adding 50 wt% EC into the solvent, the solvation structure of the electrolyte did not dramatically change, except for the appearance of EC molecules with high solubility of LiTFSI in the solvation sheaths (**Figure 2**e, right panel).[10] The 10.5 m LiTFSI in H_2O: EC (1: 1 by mass) electrolyte delivered a stability window of 2.3 V (**Figure 2**a), which is still much lower than the 3.0 V-wide window of the saturated 21 m LiTFSI in H_2O electrolyte.[5] This is due to the huge amount of free water molecules outside of the solvation sheaths that trigger preferential hydrogen evolution. In sharp contrast, when EC was introduced in the 12.5 m $LiNO_3$ in H_2O electrolyte, the electrochemical window was dramatically widened from 1.9 V to 2.7 V (**Figure 2**b), which is very close to that of the saturated 25 m $LiNO_3$ in H_2O electrolyte (2.6 V, **Figure S5**). This is because in the as-developed EC-based LWIS electrolyte (*i. e.* 12.5 m $LiNO_3$ in H_2O: EC, 1: 1 by mass), the EC molecules as diluent do not participate in the solvation sheaths due to the low $LiNO_3$ solubility in EC.[17] The increased $LiNO_3$: H_2O ratio in the EC-based LWIS electrolyte leads to an enlarged percentage of water molecules that are coordinated with Li^+, significantly decreasing the reactivity of water molecules in HER/OER. Furthermore, NO_3^- anions appear in the primary solvation sheaths of Li^+ to generate ion aggregates, reducing the water content in the primary solvation sheaths (**Figure 2**f, right panel). Likewise, the addition of PD diluent could form a LWIS electrolyte (*i. e.* 12.5 m $LiNO_3$ in H_2O: PD, 1: 1 by mass) with a similar solvation structure. However, as a protic solvent, PD can form numerous hydrogen bonds between its hydroxyl groups and the water molecules as well as NO_3^- anions, forming polymer-like chains consisting with solvation sheaths (**Figure 2**g, right panel).[18] The reactivity of water solvent in HER/OER was thereby further reduced and the electrochemical stability window was extended to 2.9 V (**Figure 2**c and **Figure S6**). For the LWIS gel electrolyte, the fluidity of electrolyte was eliminated meanwhile additional hydrogen bonds were formed between the polymer matrix and water molecules (**Figure 2**h, right panel), thus leading to a stability window as wide as 3.0 V (**Figure 2**d and **Figure S7**). This high electrolyte stability is eligible to fulfill the requirements of the electrochemical redox couple of Mo_6S_8 anode and LMO cathode. Therefore 12.5 m $LiNO_3$ in H_2O: PD gel electrolytes were selected for further investigation.

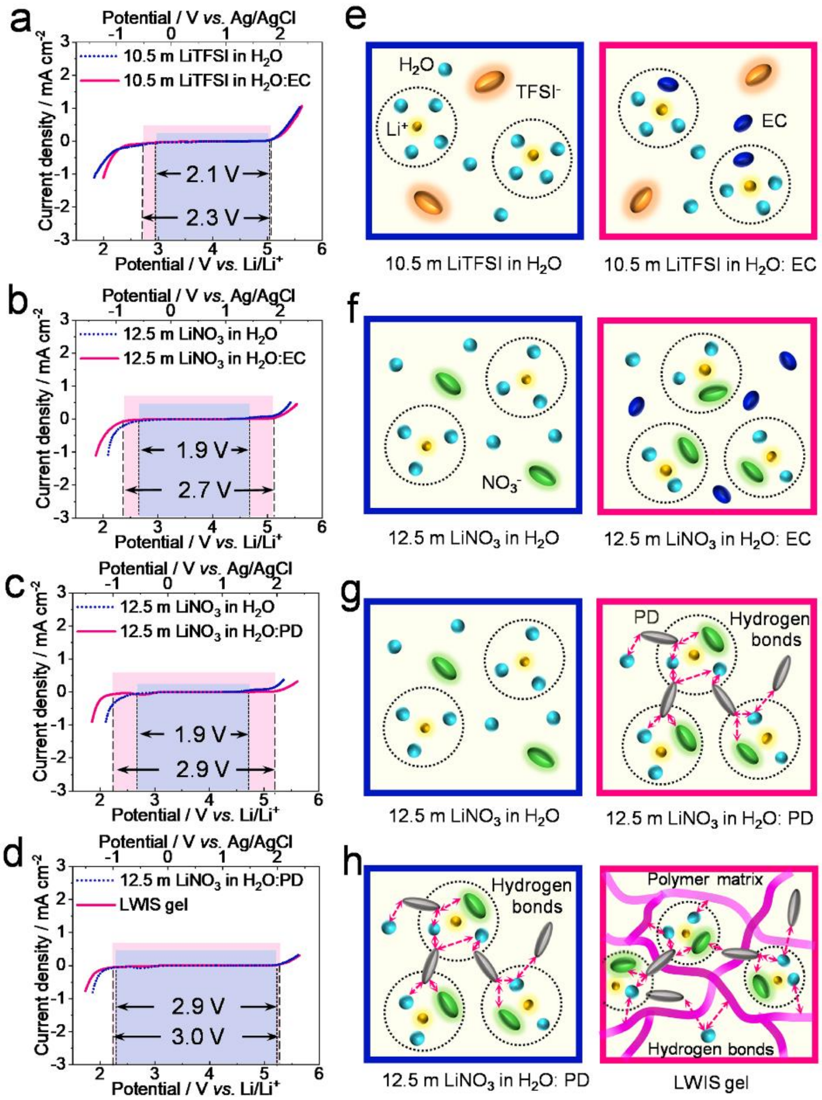

Figure 2. (**a-d**) 2nd CV curves of (**a**) 10.5 m LiTFSI in H_2O and 10.5 m LiTFSI in H_2O: EC, (**b**) 12.5 m $LiNO_3$ in H_2O and 12.5 m $LiNO_3$ in H_2O: EC, (**c**) 12.5 m $LiNO_3$ in H_2O and 12.5 m $LiNO_3$ in H_2O: PD, and (**d**) 12.5 m $LiNO_3$ in H_2O: PD and LWIS gel electrolyte couples at 0.1 mV s^{-1}. (**e-h**) The corresponding schematic hypothetical diagrams of solvation structures for the electrolytes.

Solvation structure of 12.5 m $LiNO_3$ in H_2O: PD LWIS gel electrolytes

Molecular dynamic (MD) simulations were conducted to investigate the solvation structures of 12.5 m $LiNO_3$ in H_2O: PD LWIS gel electrolytes, and compared it with two baseline electrolytes (12.5 m $LiNO_3$ in H_2O and 12.5 m $LiNO_3$ in H_2O: PD; **Figure S8**). As shown in **Figure 3**a, in the 12.5 m $LiNO_3$ in H_2O electrolyte, Li ions are mainly solvated with 4 water molecules to form a primary solvation sheath. Meanwhile, around 70 % of water molecules are coordinated with Li^+ ions, while others interact with each other via hydrogen bonds (**Figure 3**d). Such a huge amount of uncoordinated water molecules triggers significant HER reaction on the anode, which severely deteriorates the performance of the batteries.[19] Moreover, most NO_3^- ions are randomly distributed among the water molecules without any coordination with Li^+ ions (**Figure 3**a). When PD is introduced into the electrolyte, large amount of Li^+ ions prefer to partially share the primary water sheaths with the neighbouring Li^+ ions, and the Li^+ primary solvation shells are aggregated together to from polymer-like chain due to the hydrogen-bonding linkage of PD (**Figure 3**b). In such 12.5 m $LiNO_3$ in H_2O: PD LWIS electrolyte, the amount of water molecules coordinated with Li^+ dramatically increase to 94.3 %, leading to a sharp reduction of the reactivity in HER/OER for water molecules (**Figure 3**d). In particular, the number of NO_3^- anions observed in each Li^+ primary solvation sheath rises from 0.89 to 1.55 after the introduction of PD. This reduces the water number in each Li^+ primary solvation sheath, which further extends the electrochemical window (**Figure S5**). When gelling the 12.5 m $LiNO_3$ in H_2O: PD electrolyte with TEGDA monomer, the Li^+-H_2O complexes delivers a long-range aggregation. It indicates that most water molecules are immobilized by localized concentrated $LiNO_3$ salt and the polymerized TEGDA matrix (**Figure 3**c). Furthermore, as shown in **Figure 3**d, the hydrogen bonds of 12.5 m $LiNO_3$ in H_2O solution are ≈1.2 per water molecule, which significantly increases to ≈1.25 and 1.35 with the addition of PD and polymer matrix, respectively. This is mainly due to the formation of hydrogen bonds between the water molecules and NO_3^- anions in the electrolyte and the hydroxyl groups in the PD (**Figure S9**) as well as the ether groups in the polymerized TEGDA. Such water/NO_3^--PD and water-polymerized TEGDA interactions can disturb the water hydrogen bond network and further decrease the reactivity of water solvent in HER/OER, thereby effectively inhibiting the electrolyte decomposition.[20]

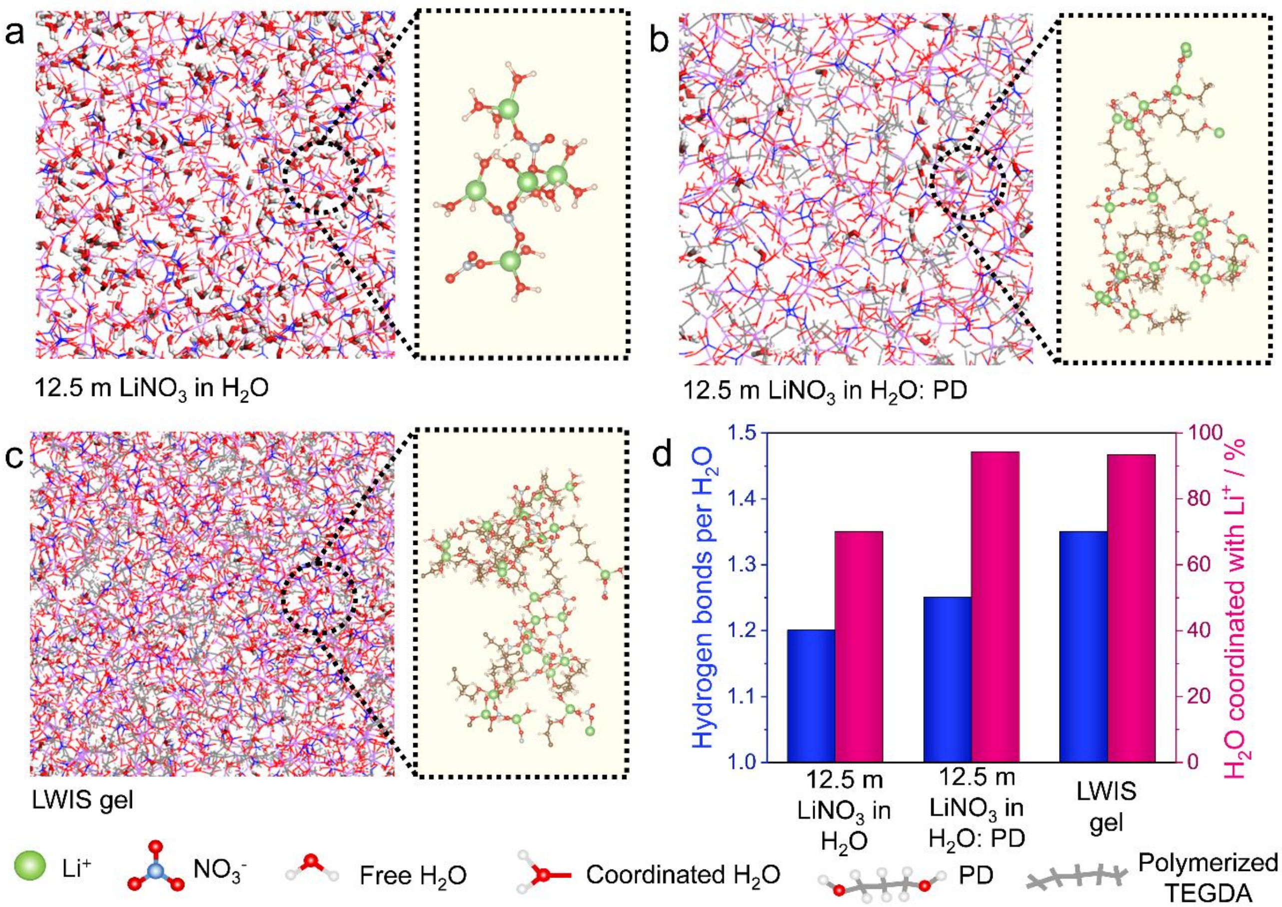

Figure 3. MD simulations of aqueous electrolytes. (**a-c**) Snapshots of the local structures of (**a**) 12.5 m $LiNO_3$ in H_2O, (**b**) 12.5 m $LiNO_3$ in H_2O: PD and (**c**) LWIS gel electrolytes obtained via MD simulation after 20 ns at 298 K. (**d**) The hydrogen bonds and the percentage of water molecules coordinated with Li^+ for three aqueous electrolyte samples at 20 ns.

Characterization of the 12.5 m $LiNO_3$ in H_2O: PD LWIS gel electrolyte

Figure 4a exhibits the polymerization mechanism of TEGDA monomer in the LWIS electrolyte. The primary radicals derived from the ultraviolet light (UV)-irradiation of 2-hydroxy-2-methyl-1-phenyl-1-propanone (HMPP) photo-initiator attack the C=C bonds of the monomer to generate free radicals. Subsequently, a chain growth reaction occurs through sequentially adding TEGDA monomer to the radical ends on the initiated monomer. Finally, a three-dimensional polymerized TEGDA network is constructed in LWIS electrolyte, and a gel electrolyte is thereby *in-situ* obtained. As shown in the right panel of **Figure 4**a, the as-prepared LWIS gel electrolyte presents an appearance of a free-standing transparent film, which can maintain its integrity under the pressure of a 100 g weight (**Figure S10**). **Figure 4**b shows the Fourier-transform infrared (FT-IR) spectra of the TEGDA monomer and polymer matrix of LWIS gel electrolyte. The peaks at ≈1245 cm^{-1} (C–O antisymmetric stretching), ≈1450 cm^{-1} and ≈1390 cm^{-1} (CH_2 bending) and ≈1720 cm^{-1} (C=O stretching) appear in the spectrum of TEGDA monomer.[21] The absorption peak at ≈1615 cm^{-1} corresponding to stretching vibration of C=C bonds disappears after polymerization, confirming a successful *in-situ* gelation of the LWIS gel electrolyte. Raman spectroscopy was employed to detect the O–H stretching vibration in different

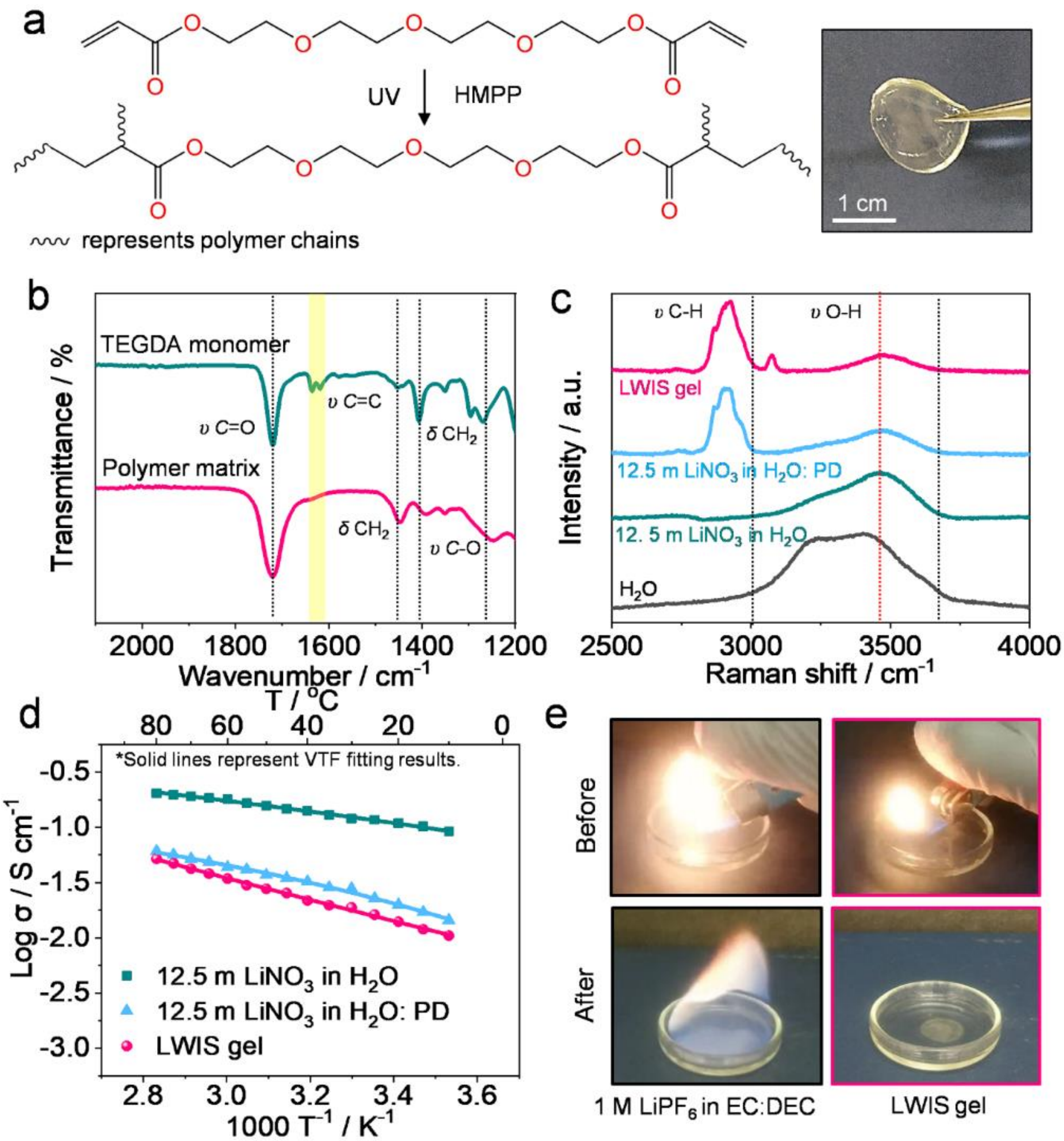

Figure 4. (**a**) In-situ polymerization mechanism of the TEGDA monomer in the presence of LWIS electrolyte. An optical image of an as-prepared LWIS gel electrolyte membrane is shown in the right panel. (**b**) FT-IR spectra of TEGDA monomer and the polymer matrix of LWIS gel electrolyte. (**c**) Raman spectra of pure water and 12.5 m $LiNO_3$ in H_2O, 12.5 m $LiNO_3$ in H_2O: PD and LWIS gel electrolytes. (**d**) Ionic conductivities of 12.5 m $LiNO_3$ in H_2O, 12.5 m $LiNO_3$ in H_2O: PD and LWIS gel electrolytes as a function of temperature. The discrete points represent the experimental data while the solid lines represent VTF fitting results. (**e**) Flammability tests of 1 M $LiPF_6$ in EC: DEC (left panels) and LWIS gel (right panels) electrolytes.

electrolytes. As shown in **Figure 4**c, the O–H stretching vibration of pure water displays a broad band centered around 3320 cm^{-1}, which is attributed to the different hydrogen-bonding environment of water molecules.[3] The intensity of this band gradually shrinks in the spectra of 12.5 m $LiNO_3$ in H_2O and 12.5 m $LiNO_3$ in H_2O: PD electrolytes, indicating that the Li^+-H_2O coordination breaks the hydrogen-bonding structure of water. The LWIS gel electrolyte exhibits a small hump at ≈3480 cm^{-1} in the Raman spectrum, which demonstrates that the free water population is dramatically diminished in this quasi-solid electrolyte. This is well-consistent with the MD simulation results in **Figure 3**.

The ionic conductivities of the different electrolyte samples were measured by electrochemical impedance spectroscopy (EIS) in a temperature range from 10 °C to 80 °C. As shown in **Figure 4**d and **Figure S11**, the plots of log σ versus T^{-1} present a non-linear Vogel Tamman-Fulcher (VTF) relationship as described by the following equation:[22]

$$\sigma = \sigma_0 T^{-\frac{1}{2}} exp(-\frac{E_a}{\mathrm{R}(T-T_0)}) \qquad (1)$$

where σ_o is a pre-exponential factor, T_o is the effective glass transition temperature, E_a is the activation energy and R is the ideal gas constant. The corresponding fitting values and ionic conductivities at 25 °C are listed in **Table S1**. The 12.5 m $LiNO_3$ in H_2O baseline electrolyte has highest ionic conductivity of 1.16 × 10^{-1} S cm^{-1} at 25 ℃, which is two-time higher than that of 25 m $LiNO_3$ in H_2O WIS electrolyte (7.38 × 10^{-2} S cm^{-1}). The low ionic conductivity of WIS electrolyte is mainly due to its huge viscosity which blocks ion transport (51 mPa s, **Figure S12**). Moreover, the crystallization of $LiNO_3$-based WIS electrolyte starts at temperature below 25 ℃, which leads to a sharp decline in ionic conductivity (from 1.73 × 10^{-2} S cm^{-1} at 20 °C to 1.60 × 10^{-5} S cm^{-1} at 10 °C, **Figure S11**). The viscosity and crystallization of $LiNO_3$-based WIS electrolyte strongly limits its practical application in batteries. After adding 50 % PD into 25 m $LiNO_3$ in H_2O electrolyte, the 12.5 m $LiNO_3$ in H_2O: PD LWIS electrolyte delivered a low viscosity (22 mPa s), which is comparable to that of the 12.5 m $LiNO_3$ in H_2O electrolyte (10 mPa s, **Figure S12**). The electrolyte crystallization was successfully inhibited in the tested temperature range attributed to the addition of PD. This results in a relatively minimal ionic conductivity change from 1.99 × 10^{-2} S cm^{-1} at 20 °C to 1.44 × 10^{-2} S cm^{-1} at 10 °C (**Figure 4**d). After polymerization, the LWIS gel electrolyte still maintains an ionic conductivity of 1.62 × 10^{-2} S cm^{-1} at 25 ℃ with a low E_a value of 2.84 × 10^{-2} eV (**Figure 4**d). This conductivity value is much higher than most of the organic liquid/gel electrolytes, and is sufficient to meet the requirements of Li-ion batteries.[23] The LWIS gel electrolyte also exhibits improved electronic insulation (**Figure S13**). Moreover, the thermal safety of LWIS gel electrolyte and conventional 1 M $LiPF_6$ in ethylene carbonate (EC): diethyl carbonate (DEC) (1: 2 by volume) electrolyte was examined via combustion tests. The LWIS gel electrolyte could not be ignited by fire sources (**Figure 4**e, right panels and **Supporting Video 1**), and the weight loss was negligible after aging in open air at 25 ℃ for 4 h (3 wt%, **Figure S14**). In contrast, the 1 m $LiPF_6$ in EC: DEC liquid electrolyte was highly flammable (**Figure 4**e, left panels and **Supporting Video 2**), and evaporated quickly at 25 ℃ (96 wt% after 4h, **Figure S14**) due to the low boiling points of the organic solvents. The superior thermal stability of the LWIS gel electrolyte facilitates safe operation of Li-ion batteries. Furthermore, the LWIS gel electrolyte can well-fill the pores of the electrodes and keep good interfacial contact with electrodes (**Figure S15** and **Table S2**).

Electrochemical performance of the Mo_6S_8||$LiMn_2O_4$ full cells using LWIS Gel electrolytes

LWIS gel-electrolytes and baseline electrolytes were compared in full cells with Mo_6S_8 anodes and LMO cathodes. CV curves of Mo_6S_8 anode and LMO cathode, and electrochemical stability window are displayed in **Figure 5**a. The Li intercalation/de-intercalation redox peaks at about 2.66 V and 3.68 V for Mo_6S_8 and the characteristic redox peaks of LMO at 4.15 and 4.29 V [5, 9] are within stability window of LWIS gel-electrolytes. However, the redox potential of the Mo_6S_8 anode is lower than the HER onset potential of pure water, 12.5 m $LiNO_3$ in H_2O and 12.5 m $LiNO_3$ in H_2O: PD electrolytes (≈2.77, 2.70, and 2.27 V *vs.* Li/Li^+, respectively, **Figure 5**b), which triggers water decomposition during the battery cycling and thus reduces the battery reversibility. In contrast, the LWIS gel electrolyte exhibits a 3.0 V-wide electrochemical window with a HER onset potential of 2.20 V *vs.* Li/Li^+, enabling the successful operation of the electrochemical redox couple of Mo_6S_8 anode and LMO cathode.

Mo_6S_8||LMO full cells with LWIS and LWIS gel electrolytes were cycled at 1 C (1 C = 122 mAh g^{-1}, based on the mass of the Mo_6S_8 anode) between 0.5 and 2.3 V (**Figure 5**c). In the cells using 12.5 m $LiNO_3$ in H_2O, a cut-off time set as 2 h was applied in the charge process to avoid continuous water decomposition. The cell suffered from severe HER at ≈2 V in the charging process (the inset of **Figure 5**c) due to 1.9 V stability window (**Figure 5**b), resulting in a low capacity of ≈25 mAh g^{-1} in the subsequent discharge (**Figure S16**a). When the salt concentration in the aqueous electrolyte was doubled to 25 m, the cell delivered an initial discharge capacity of 71 mAh g^{-1} with a Coulombic efficiency of 35 %. However, the water decomposition during cycling led to a crystallization of the aqueous electrolyte (see inset of **Figure S16**b and **Supporting Video 3**), which triggered a rapid capacity fading (34 mAh g^{-1} after 10 cycles, **Figure S16**b). The 12.5 m $LiNO_3$ in H_2O: PD LWIS electrolyte exhibited an improved cycling performance, compared with the saturated electrolyte in the full cell due to the suppression of electrolyte crystallization (**Figure S16**c). The LWIS gel electrolyte with an expanded stability window matches well with the electrode couple. As shown in **Figure 5**d, the cell showed a high initial discharge capacity of 105 mAh g^{-1} in the voltage between 0.5 and 2.3 V. The Coulombic efficiency gradually increased to 97.80 % after 20 cycles, and maintained an average Coulombic efficiency of 98.53 % over 250 cycles at 1 C (excluding the initial 20 activation cycles, whose low Coulombic efficiency could be due to the breakdown/reconstruction of SEI, irreversible proton co–intercalation in acidic electrolyte, and other complicated side reactions in the initial cycles[7, 10]). The initial Coulombic efficiency was 66.15 % for the Mo_6S_8||LMO cell (**Figure 5**d). Considering the delithiation/lithiation Coulombic efficiency of the anode was calculated to be 74.71 % based on the CV curve of Mo_6S_8 without influence of HER (**Figure 5**a), around 8.56 % of the charge capacity (*i. e.* the difference in Coulombic efficiency) could be

Accepted Manuscript

attributed to the HER in the first cycle.[24] The Mo_6S_8|LWIS gel electrolyte|LMO full cell delivered a capacity retention of 70.0 % after 250 cycles at 1 C, demonstrating an inhibited HER and stable electrolyte|electrode interfaces. The capacity fading could be due to the transition metal ion dissolution from cathode and other side reactions (*e. g.* the thickening of SEI) that consuming the limited Li inventory in the cathode. The rate performance of the cell with LWIS gel electrolyte was presented in **Figure S17**. The specific discharge capacity reached 103, 87, 75 and 25 mAh g^{-1} at 0.5 C, 1 C, 2 C and 5 C, respectively (**Figure S17**b). It is seen that the Coulombic efficiency increased with the increase of current density due to the slower side reaction kinetics at high rates (**Figure S17**a).[25] Moreover, the capacity retention was 97 % of the initial value when the current density was reversed back to 0.5 C (**Figure S17**a). Therefore, this aqueous battery configuration is highly reversible and robust. The excellent electrochemical performance of the LWIS gel electrolyte-based aqueous battery can be ascribed to the synergetic effect of PD diluent and TEGDA-based polymer matrix that efficiently reduces the water reactivity in HER/OER, and the formation of protective SEI layer on the anode that further inhibits the interfacial side reactions. The formation of SEI on Mo_6S_8 anode was confirmed by XPS analysis.

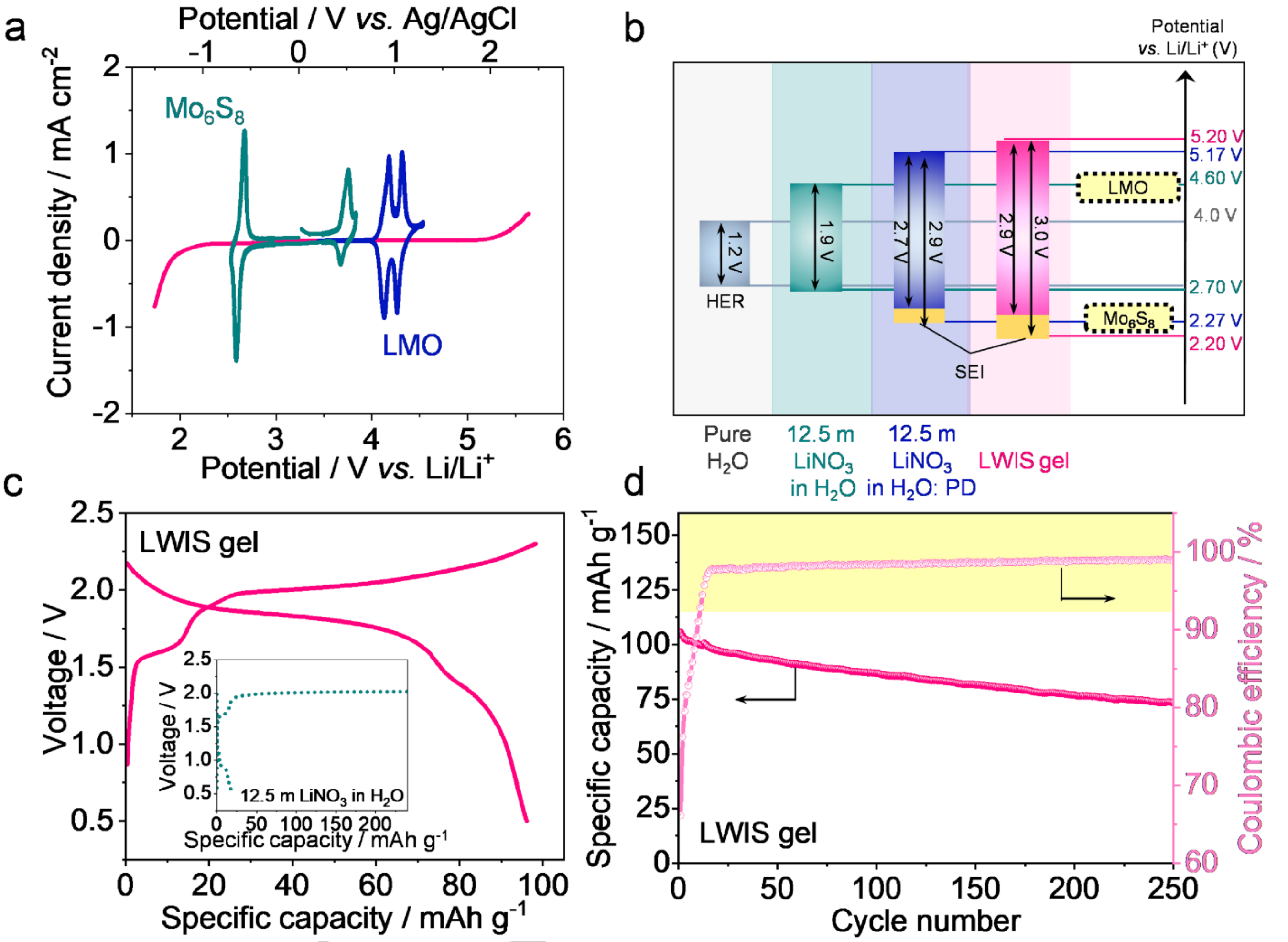

Figure 5. (**a**) CV curves of the Mo_6S_8 and LMO electrodes at 0.1 mV s^{-1} obtained with the LWIS gel electrolyte. The electrochemical window of LWIS gel electrolyte is presented for comparison. (**b**) Schematic of the electrochemical stability windows of different electrolytes and the redox voltages of Mo_6S_8 anode and LMO cathode. (**c**) Charge-discharge curves of Mo_6S_8||LMO full cells with 12.5 m $LiNO_3$ in H_2O electrolyte (inset) and LWIS gel electrolyte in the 25th cycle at 1 C. (**d**) Cycling performance of Mo_6S_8|LWIS gel electrolyte|LMO full cell at 1 C.

Formation of SEI on Mo_6S_8 anode surface in LWIS gel-electrolyte

Transmission electron microscopy (TEM) was employed to analyze the surface morphologies of Mo_6S_8 anodes after 20 cycles in different electrolytes. When the anode was cycled in 12.5 m and 25 m $LiNO_3$ in H_2O electrolyte, the Mo_6S_8 particles maintained fresh surfaces without SEI formation (**Figure 6**a and **Figure S18**a). By comparison, SEI layers with thicknesses of ≈4 nm and 7 nm were observed on the Mo_6S_8 surfaces after cycling in 12.5 m $LiNO_3$ in H_2O: PD electrolyte (**Figure S18**b) and LWIS gel electrolyte (**Figure 6**b), respectively. Moreover, these SEIs exhibited a structure consisting of Li_2O and Li_2CO_3 crystalline regions dispersed in an amorphous phase (**Figure 6**b).[26] The SEI composition was further investigated by X-ray photoelectron spectroscopy (XPS) depth profiling. For the anode cycled in LWIS gel electrolyte, peaks at about 52.3, 54.5 and 57.2 eV in the Li 1s spectra are assigned to Li_2O, Li_2CO_3 and Li_3N/LiN_xO_y species, respectively (**Figure 6**e). Meanwhile, in the O 1s spectra, peaks at around 533.8, 532.2, 530.9 and 528.7 eV correspond to N_xO_y, Li_2CO_3, C-O and Li_2O, respectively (**Figure 6**g).[27] This SEI composition is well consistent with the results of C 1s and N 1s spectra (**Figure S19**).[28] Furthermore, the outer layer of the as-formed SEI is rich in Li_2O, Li_3N and LiN_xO_y while the inner layer mainly consists of Li_2CO_3 and organic species as schematically illustrated in as **Figure 6**c. Such an organic/inorganic hybrid SEI not only effectively suppresses HER, but also possesses high strength to maintain its structural integrity. Therefore, the SEI does not break upon cycling and does not expose unpassivated surfaces, thus suppressing the interfacial side reactions (*i. e.*, HER and OER).[29] The SEI constructed in 12.5 m $LiNO_3$ in H_2O:PD electrolyte (**Figure S20**) exhibited a similar composition compared with that in LWIS gel electrolyte. The inorganic species in SEI could be attributed to the trace of dissolved N_2, CO_2 and O_2 gases in PD diluent, since their solubilities in alcohols are much higher than those in water[30] and $LiNO_3$ cannot construct any robust decomposition product layer in aqueous media;[3] Meanwhile, the organic species in SEI may be related to the reduction of PD-involved solvation shell (see **Figure S6**). For the Mo_6S_8 anode cycled in 12.5 m $LiNO_3$ in H_2O electrolyte, the Li 1s (**Figure 6**d) and O 1s (**Figure 6**f) XPS spectra displayed negligible peak intensities, confirming the SEI-free morphology on this anode. This is because the main SEI components (*e. g.* Li_2O, Li_3N, Li_2CO_3) would quickly dissolve or hydrolyze in the water media.[31] Therefore, these species can only stably exist as solid deposits on the anode surface in LWIS electrolytes with suppressed water reactivity in HER/OER. It should be noticed that recently researchers revealed that the SEI formed in aqueous electrolytes may be unstable during long cycling and storage for real-world battery application.[11, 31-32] Developing electrolyte additives and/or anode surface coating would be an attractive approach to further improve the SEI stability in the future.

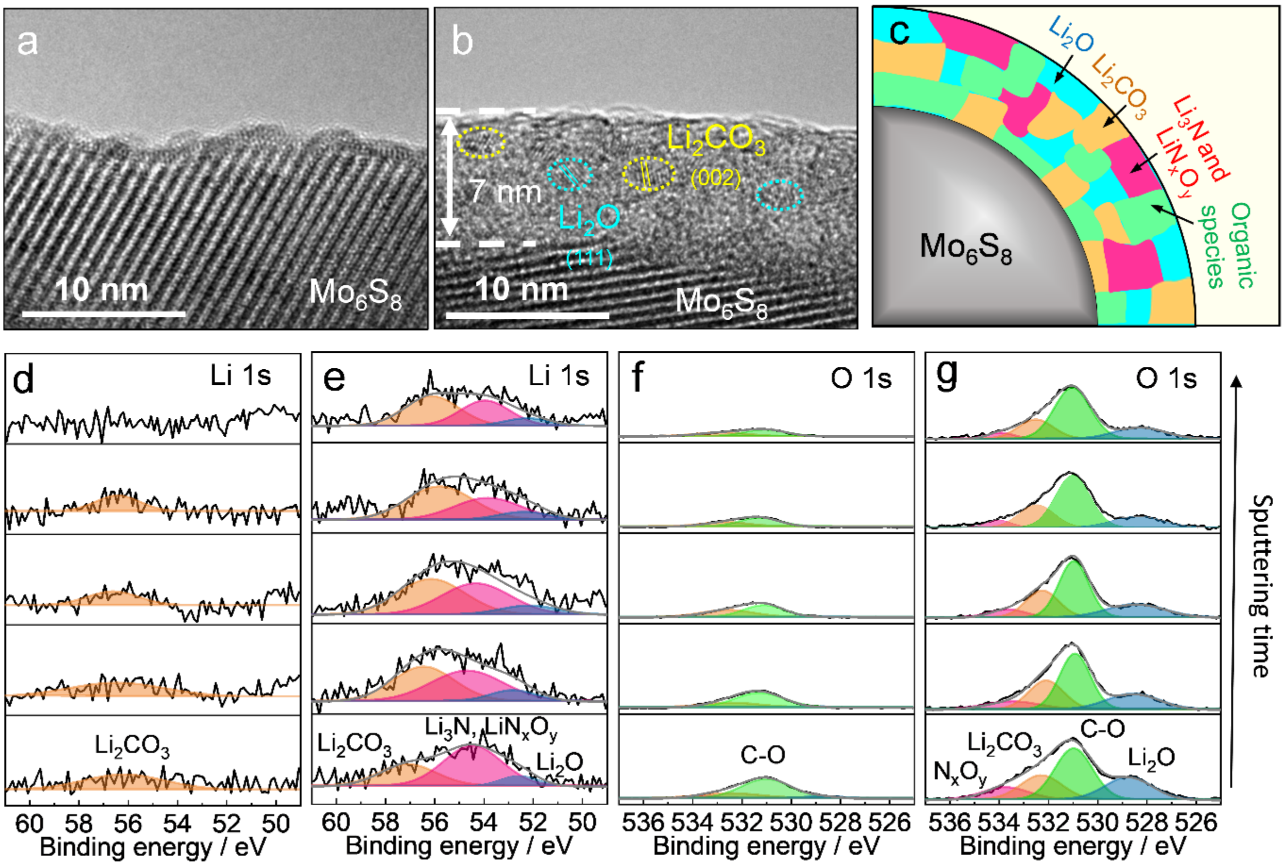

Figure 6. (**a, b**) TEM images of Mo_6S_8 anodes after 20 cycles in (**a**) 12.5 m $LiNO_3$ in H_2O and (**b**) LWIS gel electrolytes. (**c**) Schematic illustration of the SEI composition in the LWIS gel electrolyte. (**d, e**) Li 1s and (**f, g**) O 1s XPS spectra of Mo_6S_8 anode after 20 cycles in (**d, f**) 12.5 m $LiNO_3$ in H_2O and (**e, g**) LWIS gel electrolytes.

Conclusion

In summary, we reported a localized water-in-salt (LWIS) electrolyte with an electrochemical stability window of 2.9 V by using cheap inorganic $LiNO_3$ salt and 1,5-pentanediol (PD) diluent in aqueous electrolytes. The comprehensive characterizations and theoretical modelling reveal that the PD diluent not only creates a localized saturated solvation structure in the aqueous electrolyte, but also creates strong hydrogen-bonding interactions with water molecules and anions, thus significantly reducing the water reactivity in HER/OER. Furthermore, by *in-situ* gelling the electrolyte with TEGDA monomer to form a leak-free LWIS gel electrolyte, the electrochemical window was widened to 3.0 V due to further reduction of water reactivity in HER/OER and SEI formation, which is equivalent to that of the 21 m LiTFSI WIS aqueous electrolyte, but at much lower materials cost. The as-developed Mo_6S_8|LWIS gel electrolyte|LMO full cell delivered high cycling stability over 250 cycles with 98.53 % Coulombic efficiency at 1 C. The quasi-solid LWIS chemistry provides a new pathway for the development of cost-effective, safe and high-energy aqueous Li-ion batteries. Moreover, the design principles of the LWIS electrolytes can potentially be extended to a wide range of rechargeable alkali metal (*e. g.* sodium, potassium)-based and multivalent ion (*e. g.* zinc, magnesium)-based aqueous batteries for large-scale energy storage applications.

Conflicts of interest

There are no conflicts of interest to declare.

Acknowledgements

Prof. G. Wang would like to acknowledge the support by the Australian Research Council (ARC) Discovery Projects (DP200101249) and ARC Research Hub for Integrated Energy Storage Solutions (IH180100020).

Keywords: Localized water-in-salt electrolyte • aqueous lithium ion battery • 1,5-pentanediol • lithium nitrate • solid electrolyte interphase

[1] C. Yang, J. Chen, X. Ji, T.P. Pollard, X. Lü, C-J. Sun, S. Hou, Q. Liu, C. Liu, T. Qing, Y. Wang, Aqueous Li-ion battery enabled by halogen conversion–intercalation chemistry in graphite. *Nature* **2019,** *569*, 245-250.

[2] P. Jaumaux, J. Wu, D. Shanmukaraj, Y. Wang, D. Zhou, B. Sun, F. Kang, B. Li, M. Armand, G. Wang, G., Non-Flammable Liquid and Quasi-Solid Electrolytes toward Highly-Safe Alkali Metal-Based Batteries. *Adv. Funct. Mater.* **2020**, *31*, 2008644.

[3] J. Zheng, G. Tan, P. Shan, T. Liu, J. Hu, Y. Feng, L. Yang, M. Zhang, Z. Chen, Y. Lin, J. Lu, Understanding thermodynamic and kinetic contributions in expanding the stability window of aqueous electrolytes. *Chem* **2018,** *4*, 2872-2882.

[4] a) J. Xie, Z. Liang, Y.-C. Lu, Molecular crowding electrolytes for high-voltage aqueous batteries. *Nat. Mater.* **2020**, *19*, 1006-1011. b) Y. Yokoyama, T. Fukutsuka, K. Miyazaki, T. Abe, Origin of the electrochemical stability of aqueous concentrated electrolyte solutions. *J. Electrochem. Soc.* **2018**, *165,* A3299. c) L. Coustan, K. Zaghib, D. Bélanger, New insight in the electrochemical behaviour of stainless steel electrode in water-in-salt electrolyte. *J. Power Sources* **2018**, *399*, 299-303.

[5] L. Suo, O. Borodin, T. Gao, M. Olguin, J. Ho, X. Fan, C. Luo, C. Wang, K. Xu, "Water-in-salt" electrolyte enables high-voltage aqueous lithium-ion chemistries. *Science.* **2015,** *350*, 938-943.

[6] Y. Yamada, K. Usui, K. Sodeyama, S. Ko, Y. Tateyama, A. Yamada, Hydrate-melt electrolytes for high-energy-density aqueous batteries. *Nat. Energy* **2016,** *1*, 1-9.

[7] L. Suo, O. Borodin, W. Sun, X. Fan, C. Yang, F. Wang, T. Gao, Z. Ma, M. Schroeder, A. von Cresce, S.M. Russell, Advanced high-voltage aqueous lithium-ion battery enabled by "water-in-bisalt" electrolyte. *Angew. Chem. Int. Ed.* **2016,** *55*, 7136-7141.

[8] S. Ko, Y. Yamada, K. Miyazaki, T. Shimada, E. Watanabe, Y. Tateyama, T. Kamiya, T. Honda, J. Akikusa, A. Yamada, Lithium-salt monohydrate melt: A stable electrolyte for aqueous lithium-ion batteries. *Electrochem. Commun.* **2019,** *104*, 106488.

[9] Y. Shang, N. Chen, Y. Li, S. Chen, J. Lai, Y. Huang, W. Qu, F. Wu, R. Chen, An "Ether-In-Water" Electrolyte Boosts Stable Interfacial Chemistry for Aqueous Lithium-Ion Batteries. *Adv. Mater.* **2020,** *32*, 2004017.

[10] F. Wang, O. Borodin, M.S. Ding, M. Gobet, J. Vatamanu, X. Fan, T. Gao, N. Eidson, Y. Liang, W. Sun, S. Greenbaum, Hybrid aqueous/non-aqueous electrolyte for safe and high-energy Li-ion batteries. *Joule* **2018,** *2*, 927-937.

[11] L. Droguet, A. Grimaud, O. Fontaine, J.M. Tarascon, Water-in-Salt Electrolyte (WiSE) for Aqueous Batteries: A Long Way to Practicality. *Adv. Energy Mater.* **2020**.,*10*, 2002440.

[12] a) X. Ren, S. Chen, H. Lee, D. Mei, M.H. Engelhard, S.D. Burton, W. Zhao, J. Zheng, Q. Li, M.S. Ding, M. Schroeder, Localized high-concentration sulfone electrolytes for high-efficiency lithium-metal batteries. *Chem* **2018,** *4*, 1877-1892. b) Y. Yamada, J. Wang, S. Ko, E. Watanabe, A. Yamada, Advances and issues in developing salt-concentrated battery electrolytes. *Nat. Energy* **2019,** *4*, 269-280.

[13] T.A. Barnes, J.W. Kaminski, O. Borodin, T.F. Miller III, Ab initio characterization of the electrochemical stability and solvation properties of condensed-phase ethylene carbonate and dimethyl carbonate mixtures. *J. Phys. Chem. C* **2015,** *119*, 3865-3880.

[14] X. Cao, H. Jia, W. Xu, J.-G. Zhang, Localized High-Concentration Electrolytes for Lithium Batteries. *J. Electrochem. Soc.* **2021,** *168*, 010522.

[15] C. Yang, J. Chen, T. Qing, X. Fan, W. Sun, A. von Cresce, M.S. Ding, O. Borodin, J. Vatamanu, M.A. Schroeder, N. Eidson, 4.0 V aqueous Li-ion batteries. *Joule* **2017,** *1*, 122-132.

[16] T. Liang, R. Hou, Q. Dou, H. Zhang, X. Yan, The Applications of Water-in-Salt Electrolytes in Electrochemical Energy Storage Devices. *Adv. Funct. Mater.* **2021,** *31*, 2006749.

[17] C. Yan, Y.X. Yao, X. Chen, X.B. Cheng, X.Q. Zhang, J.Q. Huang, Q. Zhang, Lithium nitrate solvation chemistry in carbonate electrolyte sustains high-voltage lithium metal batteries. *Angew. Chem. Int. Ed.* **2018,** *57*, 14055-14059.

[18] a) J. Gliński, G. Chavepeyer, J.-K. Platten, Untypical surface properties of aqueous solutions of 1, 5-pentanediol. *Colloids Suf. A Physicochem. Eng. Asp.* **2000,** *162*, 233-238. b) X. Chen, Q. Zhang, Atomic Insights into the Fundamental Interactions in Lithium Battery Electrolytes. *Acc. Chem. Res.* **2020,** *53*, 1992-2002.

[19] K. Xu, C. Wang, Batteries: widening voltage windows. *Nat. Energy* **2016,** *1*, 1-2.

[20] H. Bi, X. Wang, H. Liu, Y. He, W. Wang, W. Deng, X. Ma, Y. Wang, W. Rao, Y. Chai, A Universal Approach to Aqueous Energy Storage via Ultralow-Cost Electrolyte with Super-Concentrated Sugar as Hydrogen-Bond-Regulated Solute. *Adv. Mater.* **2020**, *32*, 2000074.

[21] P. Jaumaux, Q. Liu, D. Zhou, X. Xu, T. Wang, Y. Wang, F. Kang, B. Li, G. Wang, Deep-Eutectic-Solvent-Based Self-Healing Polymer Electrolyte for Safe and Long-Life Lithium-Metal Batteries. *Angew. Chem. Int. Ed.* **2020**, *59*, 9134-9142.

[22] D. Zhou, A. Tkacheva, X. Tang, B. Sun, D. Shanmukaraj, P. Li, F. Zhang, M. Armand, G. Wang, Stable Conversion Chemistry-Based Lithium Metal Batteries Enabled by Hierarchical Multifunctional Polymer Electrolytes with Near-Single Ion Conduction. *Angew. Chem. Int. Ed.* **2019,** *58*, 6001-6006.

[23] D. Zhou, D. Shanmukaraj, A. Tkacheva, M. Armand, G. Wang, Polymer Electrolytes for Lithium-Based Batteries: Advances and Prospects. *Chem* **2019**, *5*, 2326-2352.

[24] H.-G. Steinrück, C. Cao, G. M. Veith, M. F. Toney, Toward quantifying capacity losses due to solid electrolyte interphase evolution in silicon thin flim batteries. *J. Chem.Phys.* **2020**, *152*, 084702.

[25] R.-S. Kühnel, D. Reber, C. Battaglia. Perspective - Electrochemical Stability of Water-in-Salt Electrolytes. *J. Electrochem. Soc*., **2020**, *167*, 070544.

[26] Y. Li, Y. Li, A. Pei, K. Yan, Y. Sun, C.-L. Wu, L.-M. Joubert, R. Chin, A.L. Koh, Y. Yu, J. Perrino, Atomic structure of sensitive battery materials and interfaces revealed by cryo–electron microscopy. *Science* **2017,** *358*, 506-510.

[27] W. Zhang, Z. Shen, S. Li, L. Fan, X. Wang, F. Chen, X. Zang, T. Wu, F. Ma, Y. Lu, Y., Engineering Wavy-Nanostructured Anode Interphases with Fast Ion Transfer Kinetics: Toward Practical Li-Metal Full Batteries. *Adv. Funct. Mater.* **2020,** *30*, 2003800.

[28] W. Qi, L. Ben, H. Yu, W. Zhao, G. Zhao, X. Huang, Improving the rate capability of a SiOx/graphite anode by adding $LiNO_3$. *Prog. Nat. Sci.* **2020,** *30*, 321-327.

[29] X. Cao, X. Ren, L. Zou, M.H. Engelhard, W. Huang, H. Wang, B.E. Matthews, H. Lee, C. Niu, B.W Arey, Y. Cui, Monolithic solid–electrolyte interphases formed in fluorinated orthoformate-based electrolytes minimize Li depletion and pulverization. *Nat. Energy* **2019,** *4*, 796-805.

[30] J. Tokunaga, Solubilities of oxygen, nitrogen, and carbon dioxide in aqueous alcohol solutions. *J. Chem. Eng. Data* **1975**, *20,* 41-46.

[31] N. Dubouis, P. Lemaire, B. Mirvaux, E. Salager, M. Deschamps, A Grimaud, The role of the hydrogen evolution reaction in the solid–electrolyte interphase formation mechanism for "Water-in-Salt" electrolytes. *Energy Environ. Sci.* **2018,** *11*, 3491-3499.

[32] R. Bouchal, Z. Li, C. Bongu, S. Le Vot, R. Berthelot, B. Rotenberg, F. Favier, S.A. Freunberger, M. Salanne, O. Fontaine, Competitive salt precipitation/dissolution during free-water reduction in water-in-salt electrolyte. *Angew. Chem. Int. Ed.* **2020**, *59*, 15913-15917.

Table of Contents

We present a localized water-in-salt gel electrolyte with low-cost and high safety for aqueous lithium-ion batteries. This electrolyte was fabricated by in-situ gelling TEGDA monomer in an aqueous solution based on inexpensive $LiNO_3$ salt and PD diluent. The as-developed Mo_6S_8| LWIS gel |LMO batteries delivered outstanding cycling performance in with a Coulombic efficiency of 98.53 % % after 250 cycles at 1 C.

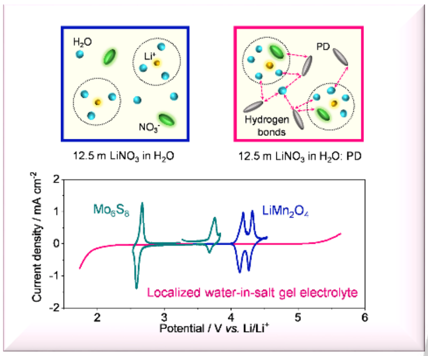

Pauline Jaumaux, Xu Yang, Bao Zhang, Javad Safaei, Xiao Tang, Dong Zhou*, Chunseng Wang*, and Guoxiu Wang*

Page No. – Page No.

“Localized Water-In-Salt” Electrolyte for Aqueous Lithium-Ion Batteries

WILEY-VCH